

# Probabilistic and deterministic full field approaches to simulate recrystallization in ODS steels

F. Villaret<sup>a,b</sup>, B. Hary<sup>b,c</sup>, Y. de Carlan<sup>b</sup>, T. Baudin<sup>c</sup>, R. Logé<sup>d</sup>, L. Maire<sup>a</sup>, M. Bernacki<sup>a,\*</sup>

<sup>a</sup> Mines-ParisTech, PSL-Research University, CEMEF – Centre de mise en forme des matériaux, CNRS, UMR 7635, CS 10207 rue Claude Daunesse, 06904 Sophia Antipolis Cedex, France

<sup>b</sup> DEN-Service de Recherches Métallurgiques Appliquées (SRMA), CEA, université Paris-Saclay, F-91191 Gif-sur-Yvette, France

<sup>c</sup> ICMMO, SP2M, Univ. Paris-Sud, Université Paris-Saclay, UMR CNRS 8182, bât.410, 91405 Orsay, France

<sup>d</sup> Thermomechanical Metallurgy Laboratory-PX Group Chair, Ecole Polytechnique Fédérale de Lausanne (EPFL), CH-2002 Neuchâtel, Switzerland

## ARTICLE INFO

### Keywords:

ODS  
Grain growth  
Recrystallization  
Monte Carlo method  
Level-set method  
Smith-Zener pinning

## ABSTRACT

Mechanical and functional properties of Oxide Dispersion Strengthened (ODS) ferritic/martensitic steels are strongly related to their microstructures. Thus, numerical modeling of microstructure evolution during ODS forming is of prime importance. In this work, two well-known full field methodologies dedicated to recrystallization modeling, the level-set and the Monte Carlo methods, are applied, discussed and compared to experimental data in their ability to describe properly recrystallization for ODS steels.

## 1. Introduction

Most of the ongoing studies about future nuclear reactor are focused on Sodium Fast Reactors (SFR) which are synonymous of severe constraints concerning the materials used in terms of stability under irradiation with or without stress, evolution under corrosive environment or ageing. Thus, new materials are needed to build these reactors and Oxide Dispersion Strengthened (ODS) ferritic/martensitic steels are, thanks to their outstanding creep and swelling resistance, one of the materials designed to complete some of these new specifications [1,2]. For nuclear applications, ODS steels are ferritic matrix steels, strengthened by a high density of Y-Ti-O oxide nanoparticles. Mechanical and functional properties of such metallic materials are strongly related to their microstructures, which are themselves inherited from thermal and mechanical processing. The understanding and modelling of microstructural evolutions, at the polycrystal scale are thus of prime importance for the control of the final in-use material properties. Ideally, numerical simulations could be used to simulate the involved mechanisms, i.e. recrystallization (ReX) and grain growth (GG) which can be potentially abnormal (AGG) [3]. However, the complex context inherent to the existence of a nanometric population of second phase particles (SPPs) makes this objective hazardous. Of course, the full field simulations of interactions between grain boundary (GB) and SPPs during GG has been extensively studied the

last decades thanks to Monte Carlo (MC) [4,5], Cellular Automaton (CA) [6], Vertex/front-tracking [7], multiphase field (MPF) [8] or level-set (LS) [9] methodologies but without clear examples dedicated to ODS steels.

A MC and a LS strategy are considered in the present article in order to reach this objective by comparing their predictions to pre-existing 2D experimental data and classical Smith-Zener predictions for ODS steels. Strengths and weaknesses of both approaches will be described. It will also be illustrated how the average size of nanoparticles can lead the Smith-Zener limit size curve to diverge from the experimental data. The 2D experimental data comes from hot extruded microstructure ODS steel bars or thermal treatment of cold formed ODS steel bars where metadynamic recrystallization (MDRX), static recrystallization (SRX) and GG mechanisms with the presence or not of SPPs were observed and quantified. The Section 2 is dedicated to the description of the used full field methodologies whereas the Section 3 described the comparisons and discussions of the obtained results with the experimental data.

## 2. Numerical frameworks concerning the full field methodologies

### 2.1. Introduction

The first metallurgical models based on the MC method have been

\* Corresponding author.

E-mail address: [marc.bernacki@mines-paristech.fr](mailto:marc.bernacki@mines-paristech.fr) (M. Bernacki).

proposed in the 1980s by Anderson and its co-workers for modelling GG kinetics [10], grain size distribution and topology [4], influence of particle dispersions [4], heterogeneous grain boundary energies [11] as well as abnormal GG [12]. Few years later, several models based on the MC approach have also been developed for post-dynamic [13,14] or dynamic recrystallization (DRX) [15,16], leading to a major improvement in terms of microstructural evolutions modelling. These schemes, based on probabilistic rules in regular grids, are advantageous in the ease of their implementation as well as their low computational cost. However, the pixelized description of the microstructure can be a problem if one needs to evaluate local grain boundary properties such as inclination or mean curvature as for other methods dealing with regular grids to describe grain interfaces. Monte Carlo step (MCS) must also be calibrated in order to be correlated with the physical time, this aspect generally requires the use of experimental data or other computational methods as it will be illustrated in Section 3.

The LS method was introduced for the first time in 1988 [17] as a numerical tool to trace the spatial and temporal evolution of interfaces. Several authors have extended this method to interfaces with multiple junctions [18,19] and a finite element level-set framework (FE-LS) for modelling of SRX mechanism in metal alloys was proposed [20,21]. Then, the LS method was used in a finite element (LS-FE) framework to model GG [22] and SRX [23] mechanisms in 2D and 3D. Dynamic recrystallization was also considered in [24,25]. Recently, the Smith-Zener pinning mechanism has also been successfully modelled in 2D [26] and 3D [27] using the LS-FE approach. Finally, very efficient LS formulation in context of regular grid and resolution thanks to Fourier transform was also considered in [28,29]. The FE-LS method has many common points with the MPF method, especially, they both avoid the difficulty of tracking interfaces and they enable a precise calculation of the mean curvature and more globally of the grain interface kinetics during recrystallization. Its use in context of classical unstructured FE mesh enables also to use it when large deformation of polycrystals are considered [25]. However, its numerical cost remains expensive and dealing with high ratio of anisotropy for the grain boundary energy or mobility is not straightforward [30].

## 2.2. Level-set method

In this work, the full field modelling was performed by using the LS method in a P1 FE framework and a MC method on a regular grid. Details of the used LS methodology can be found in [31] and only the main elements are recalled here. In the LS approach, each sub-domain  $G$  (grain) in a given domain  $\Omega$  (polycrystal) is described in an implicit way by computing a signed distance function  $\phi(x, t)$  representing the distance to the sub-domain boundaries  $\Gamma = \partial G$  (grain boundaries). In the considered P1 framework,  $\phi(x, t)$  is evaluated at each node on the FE mesh and is chosen, by convention, negative outside of the grain and positive inside:

$$\phi(x, t) = \pm d(x, \Gamma(t)), x \in \Omega, \quad (1)$$

$$\Gamma(t) = \{x \in \Omega: \phi(x, t) = 0\}, \quad (2)$$

with  $d(x, \Gamma(t))$  the Euclidean distance from the point  $x \in \Omega$  to the boundary  $\Gamma(t)$ . In the LS method, the evolution of  $\phi(x, t)$ , submitted to a velocity field  $\vec{v}(x, t)$  is then given by the following convective partial differential equation [17]:

$$\frac{\partial \phi(x, t)}{\partial t} + \vec{v}(x, t) \cdot \nabla \phi(x, t) = 0, \quad (3)$$

$$\phi(x, t = 0) = \phi^0(x). \quad (4)$$

The kinetic law for grain boundary motion in polycrystals at the mesoscopic scale is classically defined as [32]:

$$\vec{v} = MP\vec{n}, \quad (5)$$

with  $M$  the grain boundary mobility,  $P$  the net pressure i.e. the net driving force per unit area, and  $\vec{n}$  the outward unit normal to the GB. In context of LS approach and by neglecting torque terms [30], the net pressure is classically defined as:

$$P = \tau[\rho] - \gamma\kappa, \quad (6)$$

with  $\tau$  the dislocation line energy,  $[\rho]$  the dislocation density jump across interfaces,  $\gamma$  the interface energy and  $\kappa$  the mean interface curvature (i.e. the curvature in 2D and the sum of main curvatures in 3D). The isotropy hypothesis remains here, for the LS simulations, to consider  $\gamma$  as constant and  $M$  as only dependant of the temperature through an Arrhenius law  $M = M_0 \exp(-Q/RT)$  with  $M_0$  a pre-exponential constant parameter,  $R$  the gas constant and  $T$  the absolute temperature. By using coloring/recoloring algorithms [33] and some metric properties of the LS functions, one can solve, for  $N_g$  grains, a set of  $N_p$  convective-diffusive equations as detailed by Eq. 9, with  $N_p \ll N_g$ , to take into account Eq. (5) for all the grains of the considered polycrystal. The numerical strategy consisting in limiting the number of involved LS functions is crucial in terms of numerical cost.

$$\frac{\partial \phi_i(x, t)}{\partial t} - M\gamma\Delta\phi_i(x, t) + \vec{v}_i^{[\rho]} \cdot \nabla \phi_i(x, t) = 0, \quad (7)$$

$$\vec{v}_i^{[\rho]} = M\tau[\rho]_i \vec{n}_i, \quad (8)$$

$$\phi_i(x, t = 0) = \phi_i^0(x). \quad (9)$$

Moreover, a classical numerical treatment at multiple junctions, proposed in [18] and detailed by Eq. 10 is used at each time step after solving the convective-diffusive Eq. (7) in order to avoid kinematic incompatibilities.

$$\phi_i(x, t) = \frac{1}{2}(\phi_i(x, t) - \max_{j \neq i} \phi_j(x, t)), \quad 1 \leq i \leq N_p. \quad (10)$$

Finally, as detailed in [22], the adopted numerical formulation implies to work with distance functions (i.e. to deal with LS functions respecting the Euclidean metric). Thus a parallel and direct reinitialization algorithm detailed in [34] is used at each time step after solving Eq. 10.

All the details concerning different strategies to define the jump of dislocation density  $[\rho]$  and the subsequent  $\vec{v}_i^{[\rho]}$  can be found in [31]. Here, as illustrated in Section 3.4, the dislocation density field will be defined directly thanks to experimental data, and averaged per grain, as detailed in [35].

The convection-diffusion equations (Eq. (7)), under zero Neumann boundary condition and the definition of a common global velocity field as detailed in [20], are solved in the following by using an implicit streamline upwind Petrov-Galerkin FE scheme.

It has been proven [26], that the proposed formalism is able to deal with static SPP and the resulting Smith-Zener pinning effect without any assumption concerning the interactions between particle and grain interfaces. This ability will be used in the present works.

## 2.3. Monte Carlo method

Monte-Carlo (MC) method is based on probability theory: microstructure evolutions are modelled by calculating probability laws minimizing an estimation of the system's energy. The whole domain is discretized in a finite number of cells (pixels in 2D or voxels in 3D) called sites. A crystallographic orientation is defined with the three Euler angles from an experimental EBSD map on each pixel with the method proposed by Baudin et al. in [36]. For this study, grains and sub-grains are delimited by interfaces between two pixels disoriented for more than  $10^\circ$  and  $2^\circ$  respectively (these values are generally dependent of the considered material). The sub-routine used to compute this misorientation comes from the works of Wang et al. [37].

At each Monte Carlo Step (MCS),  $N$  pixels (with  $N$  the total number of pixels) are randomly picked for a potential reorientation to the orientation of a neighbouring pixel. A same pixel could be picked several times. First, interface energy ( $\gamma(\theta_{ij})$ ) is calculated between two neighboring sites, using the Read-Schockley equation [38], defined as:

$$\gamma(\theta_{ij}) = \begin{cases} \gamma & \text{for } \theta_{ij} \geq 10^\circ \\ \gamma \times \frac{\theta_{ij}}{10} \left(1 - \ln \frac{\theta_{ij}}{10}\right) & \text{for } \theta_{ij} < 10^\circ \end{cases} \quad (11)$$

where  $\theta_{ij}$  is the misorientation between the pixels  $i$  and  $j$  and  $\gamma$  the interface energy for highly misoriented boundaries ( $\geq 10^\circ$ ). The total interface energy of the pixel  $i$ ,  $Ec_i$ , is defined as the sum of each interface energy by considering the  $N_i$  first neighbors [37]:

$$Ec_i = \sum_{j=1}^{N_i} \gamma(\theta_{ij}). \quad (12)$$

An energy variation  $\Delta Ec_i$  is defined when the pixel  $i$  changes its orientation to the orientation of one neighbouring pixel as:

$$\Delta Ec_i = \frac{1}{L} \left( Ec_i^{\text{initial}} - Ec_i^{\text{final}} \right), \quad (13)$$

where  $L$  is a characteristic length used for units homogeneity: stored energy and pinning energy are volume energies written in  $J \cdot m^{-3}$  and surface energy is expressed in  $J \cdot m^{-2}$ . Most of the authors in literature are not using this units homogenization, because they are either using dimensionless energy levels or because the modelled mechanism implies only surface energy (such as GG without particles or with particles modelled by chosen sites). This constant need to be well chosen: its value controls the balance between volume and surface energies and so simulations results such as the limit grain size due to the presence of SPP. For this study,  $L$  was fixed at  $1 \mu\text{m}$  to be close from the initial mean grain size. For pixels coming from grains with a size under the mean grain size, the capillarity pressure will be underestimated compared to volume forces, and for pixels from grains with a size above the mean grain size, it will be overestimated. However, standard deviation of grains size distribution is relatively low for the considered microstructures, so the impact of  $L$  on balance between surface and volume energy is limited.

Stored energy could also be considered on each pixel, the stored energy variation induced by the reorientation of a pixel  $i$  to the orientation of his neighbouring pixel  $k$  is defined as:

$$\Delta Es_{ik} = (Es_k - Es_i) = 0.5Gb^2(\rho_{dk} - \rho_{di}), \quad (14)$$

where  $G$  corresponds to shear modulus,  $\rho_{dk}$  to the dislocation density of the pixel  $k$  and  $b$  to the Burger's vector.

In the traditional MC approach, second phase particles are represented by pixels with a specific orientation [4,14]. These sites could not be reoriented, so particles are constant in size and immobile. This method is a rough approximation of the real interactions between particles and the grain boundaries.

In ODS steels, oxide particles are generally so small that this method is not adapted: sites sizes (which is classically equal to the step used for EBSD indexation), is much higher than particles size. That is why, for this study, another approach developed by Eivani et al. [39] to incorporate the effect of small oxides, is used. In this method, particles populations are analytically described on each site with a constant  $Ez_i$ , which represent the Smith-Zener pinning energy induced by the particles:

$$Ez_i = Pz_i = \frac{3f_i\gamma(\theta_{ij})}{2r_i}, \quad (15)$$

where  $f_i$  is the volume fraction and  $r_i$  the mean radius of particles on the considered pixel  $i$ . A normal distribution of particles radii is generally used to get closer from real materials.

It must be highlighted that the use of the Smith-Zener pressure

model implies an important number of strong hypothesis concerning the interactions between the SPP and the grain boundaries. The limit of a such approximation in context of real second phase particle populations was already illustrated [27]. Moreover, one of the assumptions implied by the Smith-Zener's approach consists to consider the grain interface thickness as negligible comparatively to the SPP mean size, which could be, of course, not acceptable in context of ODS steels. So, this model must be used carefully when dealing with nanoparticles.

At the end, before testing the reorientation, these energy contributions are summed up on each pixels:

$$\Delta E_{tot_i} = \Delta Ec_i + \Delta Es_{ij} + Ez_i, \quad (16)$$

and reorientation probability rules minimizing the system energy are calculated as follow:

$$P_{i \rightarrow j} = \begin{cases} \frac{M(\theta_{ij}) \frac{1}{L} \gamma(\theta_{ij}) + \Delta Es_{ij}}{M_m \frac{1}{L} \gamma + Es_i} \exp\left(-\frac{\Delta E_{tot_i}}{kT}\right) & \text{if } \Delta E_{tot_i} > 0 \\ \frac{M(\theta_{ij}) \frac{1}{L} \gamma(\theta_{ij}) + \Delta Es_{ij}}{M_m \frac{1}{L} \gamma + Es_i} & \text{if } \Delta E_{tot_i} \leq 0 \end{cases} \quad (17)$$

when energy is minimized ( $\Delta E_{tot_i} \leq 0$ ), reorientation probability is proportional to grain boundary mobility  $M(\theta_{ij})$ , which is considered anisotropic and dependent on the temperature and the misorientation angle:

$$M(\theta_{ij}) = \begin{cases} M_m = M_0 \exp\left(-\frac{Q}{kT}\right) & \text{for } \theta_{ij} \geq 10^\circ \\ M_m \left(1 - \exp\left[-\left(\frac{\theta_{ij}}{10}\right)^3\right]\right) & \text{for } \theta_{ij} < 10^\circ \end{cases} \quad (18)$$

where  $Q$  corresponds to the activation energy.

When energy is not minimized ( $\Delta E_{tot_i} > 0$ ), reorientation probability is very low, but not zero. The exponential factor ( $\exp\left(-\frac{\Delta E_{tot_i}}{kT}\right)$ ) corresponds to thermal agitation, and avoid artificial lattice pinning [40]. Therefore,  $kT$  is an adjustable parameter which need to be calibrated with experimental values.

In the Monte Carlo model, the link between the MCS and the physical time is not straightforward. As detailed, one MCS is reached when then number of pixels selected for a potential reorientation is equal to the number of pixels on the whole domain and a given pixel can be selected several times or never.

In the following, cell size was fixed by a convergence study of the MC predictions. Since the MC model is based on relatively simple probability calculation on regular grid, calculation times are reasonable (few hours to one day for the considering test cases in single-processor calculations). Another interesting aspect of this model is the possibility to introduce easily crystallographic texture and anisotropic grain boundary data (dependent of the misorientation but not of the inclination). The absence of a direct link with physical time and the use of purely numerical parameters (such as the kinetic parameter  $kT$  or the Smith-Zener pressure to describe pinning effects), constrain to calibrate finely the model with numerous experimental results. We will also illustrate in the next section the possibility to calibrate MC simulations thanks to FE-LS results.

### 3. Results and discussions

All simulations were realized for isothermal treatments. .

#### 3.1. Comparisons between MC and LS models for GG phenomenon without SPP

In this section, GG simulations at  $T = 1423.15$  K were performed with polycrystals immersed from experimental EBSD data (Fig. 1). Interfaces defining grains boundaries required for the LS method and grain size measurements were defined with a threshold of  $2^\circ$  on the

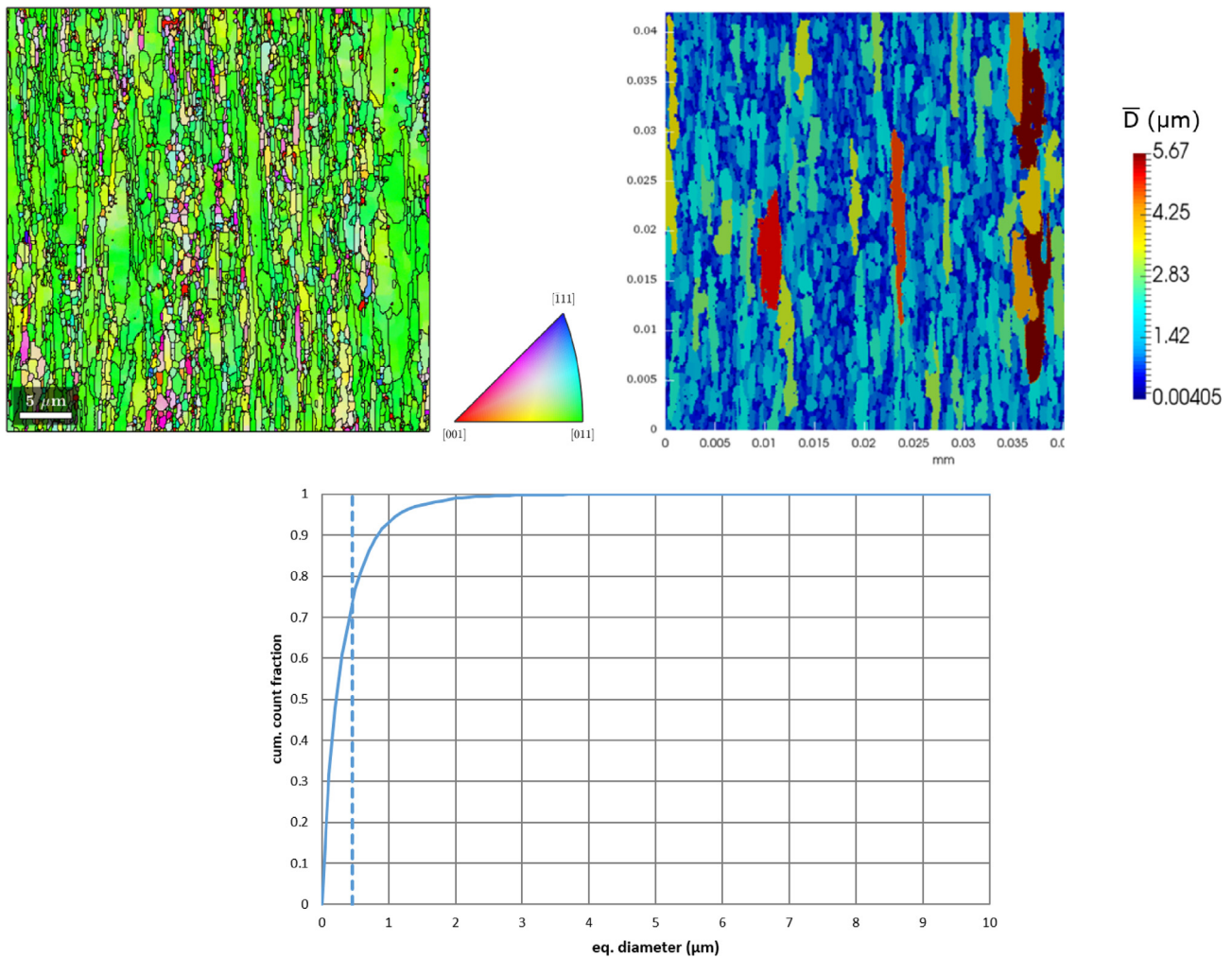


Fig. 1. Top left: initial experimental EBSD map used for MC simulations. Top right: initial polycrystal, immersed from the EBSD map and used for LS simulations. Bottom: initial grain size distribution, the dashed line correspond to the initial mean grain size.

misorientation between two neighboring pixels. Considering this threshold the simulation domain contains about 1600 grains. Simulations were stopped before the number of grains becomes too low in order to avoid boundary effects.

For this case, LS simulation was realized on a mesh containing about 162 200 elements whereas the MC simulation was realized on the experimental map ( $20 \times 20 \mu\text{m}^2$ ) containing 31 862 pixels. In MC and LS simulations, interface energy is set to  $\gamma = 0.79 \text{ J} \cdot \text{m}^{-2}$  [41], activation energy is set to  $Q = 174 \text{ kJ} \cdot \text{mol}^{-1}$  and grain boundary mobility is set to  $M_0 = 4.7 \times 10^{-6} \text{ m}^4 \cdot \text{J}^{-1} \cdot \text{s}^{-1}$ .  $M_0$  was experimentally estimated in [42].

In order to compare microstructure evolutions from LS and MC simulations at the same time, it is required to perform a time calibration, i.e. giving at each MCS a corresponding time value from the LS method. This conversion (Fig. 2) was obtained by comparing equivalent mean grain diameter,  $2\bar{R}$  (evaluated in number), at given MCS with LS results. A linear relationship is obtained, with an equivalence of almost 171 MCS for 1 s.

Using this relationship, it is possible now to compare microstructure evolutions and grain size distributions at different times (Fig. 3).

Grain maps and size distributions between MC and LS models are very similar independently of the considered time. These results illustrate that pure GG could be described either by solving partial differential equations or by probability laws minimizing system energy. Then, it is also possible to use easily a LS method as a reference for MC kinetics. In this case, it is possible to describe the crystallographic texture evolution with the MC method (Fig. 3 bottom left) and compare

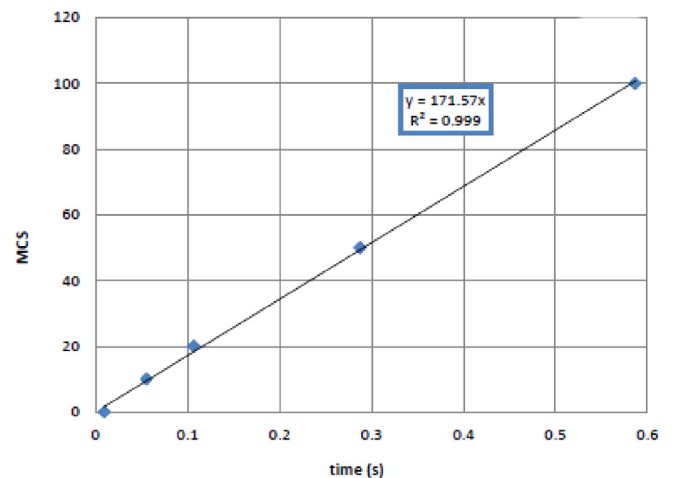


Fig. 2. Relationship between MCS and time obtained by equivalent mean grain diameter comparisons between LS and MC results.

it to experimental data (Fig. 4).

### 3.2. Grain growth with particles, comparisons with the Smith-Zener model

In these simulations, particles were introduced to measure their

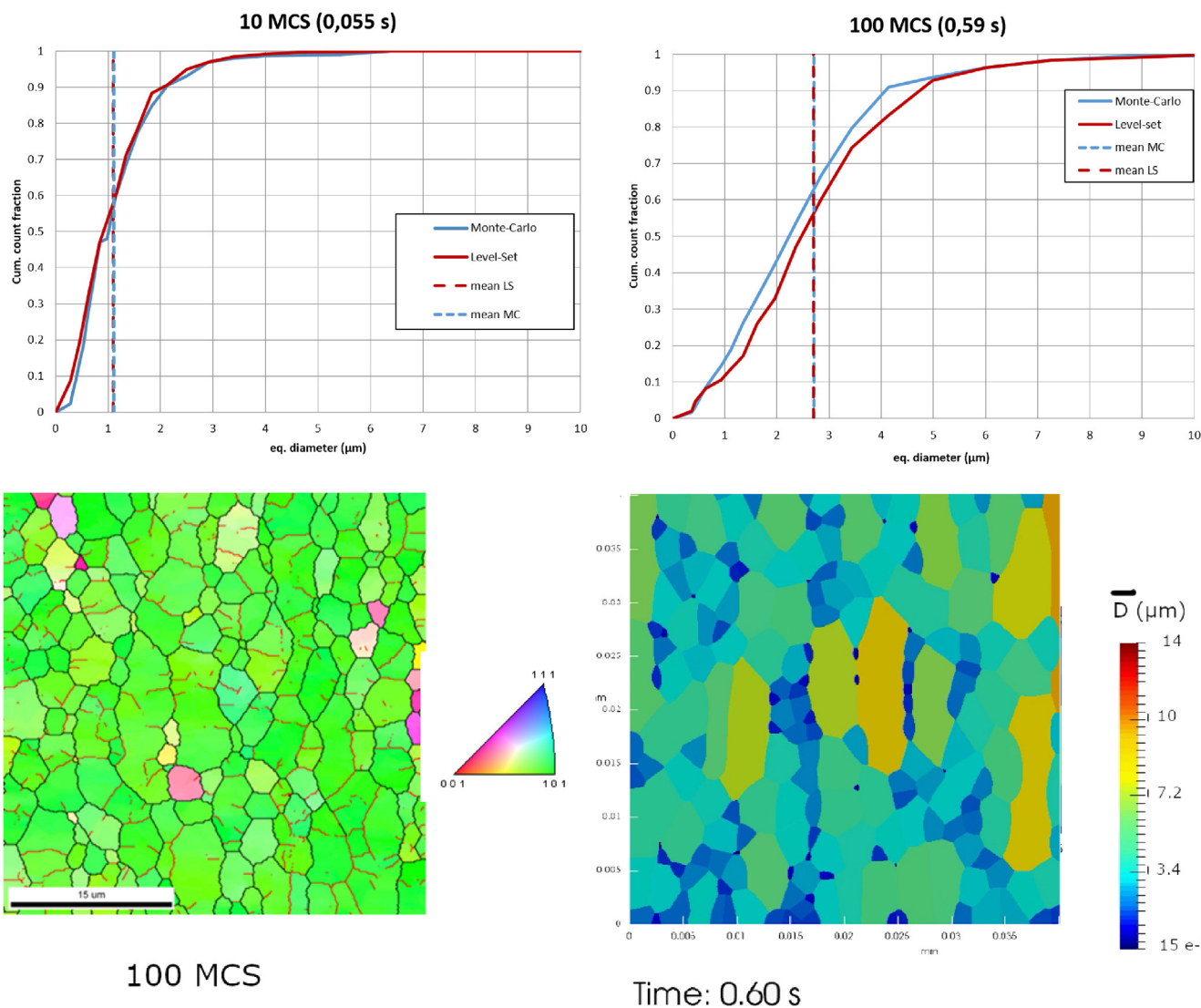


Fig. 3. Comparisons of microstructures evolutions - top: grain size distributions (equivalent diameter in number) from MC (blue) and LS (red) simulations at different times. The vertical dashed lines describe mean values of the distributions. Bottom: MC (left side) and LS (right side) maps at 0.6 s (100 MCS).

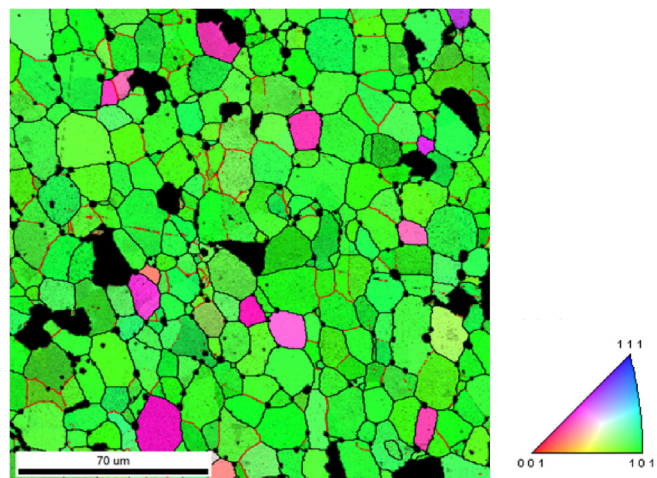


Fig. 4. Experimental EBSD map obtained on a hot extruded bar after heat treatment at 1575.15 K during 1 h [42].

effect on microstructure evolutions (known as Smith-Zener pinning effect). In ODS steels, particles diameter is usually ranging from 1 nm to 10 nm [43], and it could reach values above 1 μm if particles coarsen. That is why particles cannot be indexed on an EBSD map, Scanning Electron Microscope (SEM) resolution is too low and the scale difference between grains and particle is too large. To face this problem, particles were randomly distributed on microstructure for LS simulations. In order to get closer from the reality, a normal distribution was defined for particles radius with  $\bar{r}$  the mean particles radius and a dispersion  $\sigma = 3.3$  nm. This problem is simplified in MC method by using a slowing force from the Smith-Zener model (see part 2.3). This is why there is an interest in comparing the predictions obtained with a deterministic simulation where particles are explicitly represented, such as LS method, with the one where particles are introduced thanks to mean laws, such as the proposed MC simulations.

Different particle sizes (and so different temperatures) and surface fractions were simulated for these comparisons (see Table 1). Simulations number from 2 to 5 aim to compare the obtained limit grain size with MC simulations and the Smith-Zener model. Simulations 6 and 7, with bigger particles, aim to compare the LS simulated limit grain size with experimental data. Even if in ODS steels, particles radius is usually smaller than 5 nm (1–2 nm in Ti enriched ODS steel), LS simulations with such particles size were not carried out in this study because of the

**Table 1**  
Numerical experiment plan.

Simulation Id <sup>a</sup>	1	2	3	4	5	6	7
mean particles radius (nm)	–	10	10	5	5	950	600
particles surface fraction %	0	1	0.5	1	0.5	3.4	2.5
Temperature (K)		1423.15					1575.15

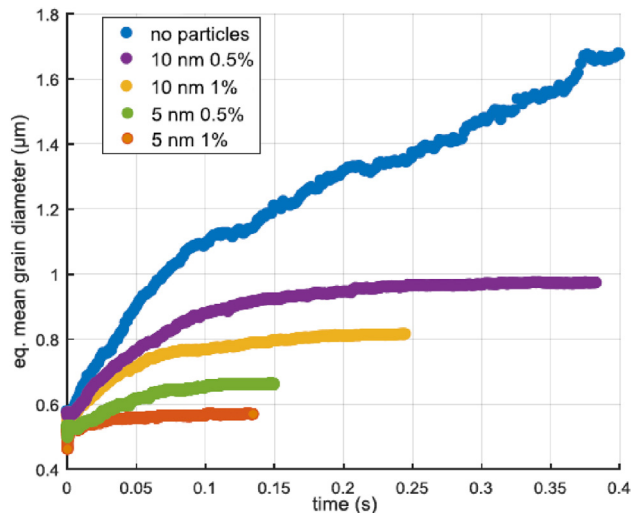


**Fig. 5.** Evolution of equivalent mean diameter for different particles radii and surface fraction (LS method, simulations 1–5).

numerical limits in terms of FE mesh size and also because particle size would be on the same order of magnitude of the grain boundary thickness which is defined as a sharp interface in LS formalism. More globally, this assumption (grain boundary thickness negligible comparatively to the particle equivalent size) is also a basic assumption of the Smith-Zener pressure mean field model. So, considering Eq. 15 in such context for MC model is questionable and must be used carefully.

As expected, introducing SPP slows down GG by pinning effect, until it stops at a maximum grain size (Fig. 5). The final grain size depends on the size and number (surface fraction) of particles: for a high number of particles (such as orange curve in Fig. 5) the microstructure shows almost no evolution, initial grain size is quite equal to the limit grain size. The same microstructure with a lower number of particles (purple curve on Fig. 5) shows grain growth until the final grain size is reached.

Well-known Smith-Zener model is often used to predict a limit grain size when grain boundaries can be assumed discrete comparatively to the particle size. A retaining force named Zener or Smith-Zener pressure (see Eq. 15), can be generalized to real cases by adding constant parameters ( $k$  and  $m$ ). When the limiting grain size is reached, grains boundary motion is stopped and the Smith-Zener pressure is then equivalent to the capillarity forces, it could be written:

$$\frac{2\gamma f^m}{k\bar{r}} = \frac{2\gamma}{\bar{R}_{lim}} \Leftrightarrow \bar{R}_{lim} = \frac{k\bar{r}}{f^m}. \quad (19)$$

With this model, for a given particles surface fraction  $f$ ,  $\frac{\bar{R}_{lim}}{\bar{r}}$  should be a constant value. Fig. 5 and Fig. 6 illustrate that it is not the case for ODS steels: for a constant  $f = 0.5\%$  (purple and green curves), dividing  $\bar{r}$  by 2 (from 10 nm to 5 nm) does not imply dividing  $\bar{R}_{lim}$  by 2: for purple curve  $\bar{R}_{lim} = 0.97 \mu\text{m}$  and for green curve  $\bar{R}_{lim} = 0.66 \mu\text{m}$  instead of  $0.48 \mu\text{m}$  which represent a shift of 36%. An explanation of this shift in the limit grain size comes, of course, of the strong hypothesis behind the Smith-Zener model, which are generally not respected [27]. For example, in the considered context the hypothesis "grain boundaries are not deformed by particles contact" is not valid. Even if this model seems

not well respected, points from LS simulations could be plot with experimental results measured with  $\bar{r}$  smaller than 5 nm (see Fig. 6).

For high surface fraction and big particles size (right part of the curve, see Fig. 6), experimental data and LS simulations are in excellent agreement. It means that materials parameters (mobility  $M$  and interface energy  $\gamma$ ) are well approximated, and that grain boundary anisotropy and 3D effects seem to have a limited impact for this kind of pinned microstructure.

For small surface fraction and small particles size (left part of the curve), experimental points are no longer on the power law curve extrapolated from LS simulations. This result suggests that for these microstructures, other parameters should be considered in the numerical framework and/or that Smith-Zener framework is not well adapted for such size of nanoparticles. This statement is in line with the state of the art where it was already illustrated that small particles could be fully/partially cut through the grain boundary migration leading to a limited pinning effect of second phase particles [44].

### 3.3. Grain growth with particles, comparisons between MC and LS models

Results from simulations 2 and 3 (see Table 1) are compared with MC simulations. First of all, it is interesting to check if the relationship found in part 3.1 to link MCS and physical time remains the same when particles are added. In the same way as in part 3.1, a correlation between MCS and LS time was set by comparing mean equivalent diameter (see Fig. 7).

After 2 MCS, microstructures are quite totally pinned, especially for  $f = 1\%$  (blue diamond on Fig. 7), so only few points could be used for comparisons with LS simulations, moreover the limit mean grain size obtained with MC predictions is lower than one obtain with LS ones (see Table 2). In consequence, the link between MCS and time is linear only at the very beginning of the simulation as it is illustrated in Fig. 7. (see Table 3).

The relation between MCS and time is quite the same for these two cases with particles. Few more MCS are needed for the same heating time than for case without particles (around 170 MCS for 1 s, Fig. 2) which means that particles modelled by a Smith-Zener force are slowing down kinetics in MC simulations. The shift observed at the origin between time and MCS on Fig. 7, could be explained by the non-indexed pixels treatment which is different in the two methods. Indeed, in the MC method, non-indexed pixels are treated apart from the others: a default orientation is set and they could not be used to reorient a neighbor pixel, so they are not counted in statistics. In the LS method used here, non-indexed pixels are treated in the same way as other: as they have a default orientation they are considered as very small grains, so they are counted in statistics which leads to a lower value of mean equivalent radius (evaluated in number) only at the first increments as they then naturally disappear by the curvature flow. This shift could be increased by the particles: more the pinning effect is high, more grains boundaries are slowed down and more the non-indexed pixels stay for long. Without particles this shift is almost invisible (Fig. 2).

Fig. 8 shows the comparison between MC and LS microstructures at pinned state. These two models leads to small-grained microstructure because of the particles pinning. This figure shows also two main differences of these models: in the LS methods, particles are explicitly represented so they are visible on the microstructure (very small white dots), but these simulations are not considering grain orientation unlike the MC method. Table 2 and Figs. 9 compares grain sizes from these maps. Mean grain sizes at pinned state are close but there relative deviation is not negligible (see Table 2). This reasonable deviation could be an effect of the non-physical parameter  $L$  introduced in the MC model (see Section 2.3). Indeed, the initial grain size  $D_{ini}$  is around  $0.45 \mu\text{m}$  for this simulation, so  $L$  is slightly higher than  $D_{ini}$ , leading to a small underestimation of the capillarity in comparison to the pinning pressure. Considering this shift in the mean, grain size distributions are relatively close from each other no matter which is the considered

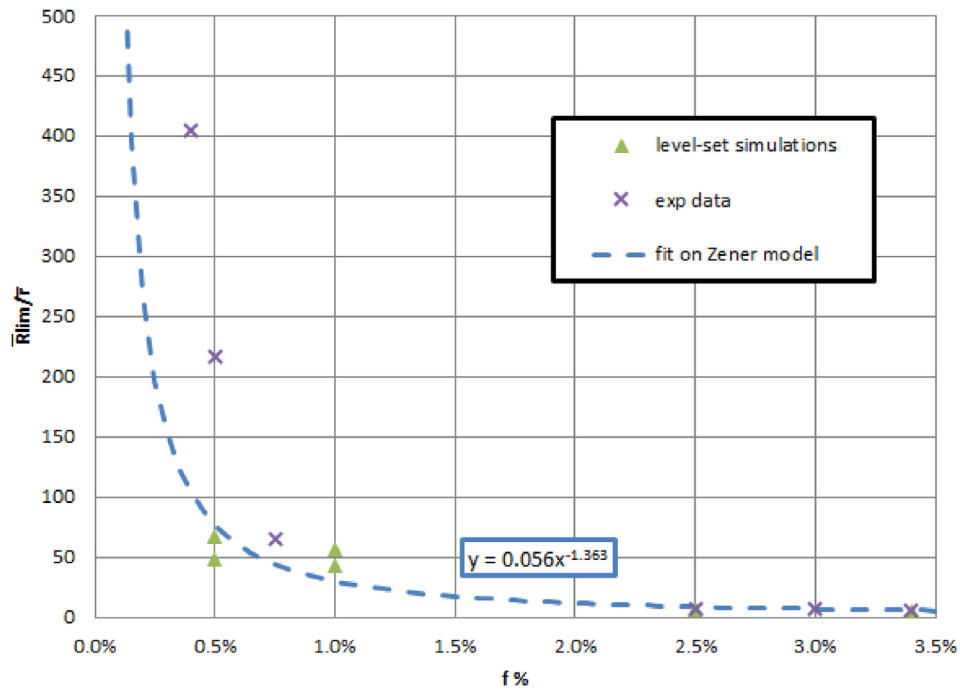


Fig. 6. Fit on the Smith-Zener model with simulation results (triangles) and comparisons with experimental data from [42].

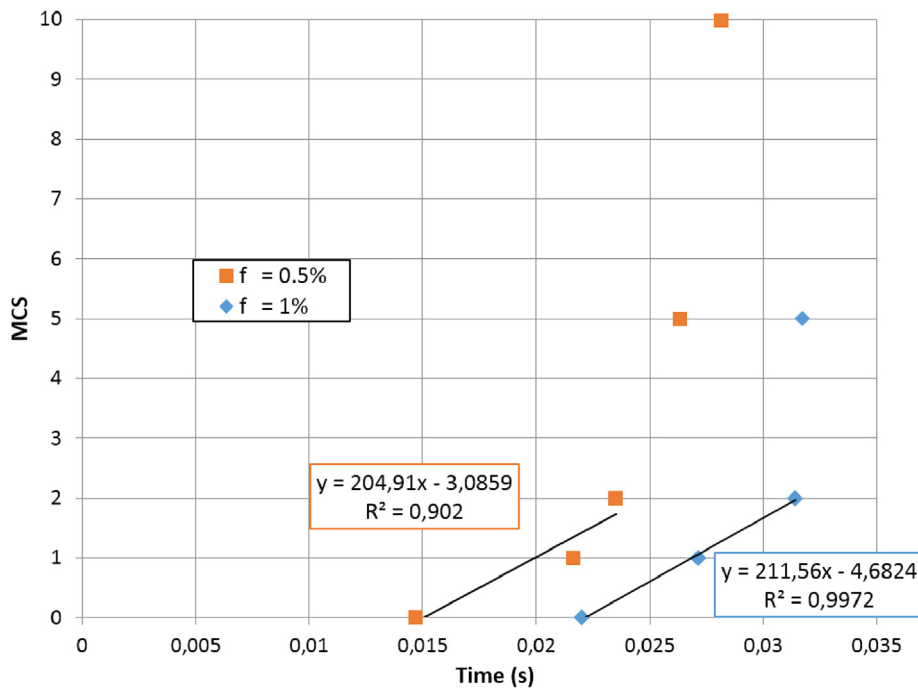


Fig. 7. Relationship between MCS and time obtained by equivalent mean grain diameter comparisons between LS and MC results for grain growth with particles ( $F = 10 \text{ nm}$ ).

Table 2  
Mean grain size at pinned state obtained with MC and LS simulations.

$\bar{r}, f$	$D_{lim} (\mu\text{m})$ in MC	$D_{lim} (\mu\text{m})$ in LS	relative deviation $\left(\frac{LS-MC}{LS}\right)$
10 nm, 0.5%	0.75	0.93	19%
10 nm, 1%	0.7	0.82	15%

Table 3  
Numerical experiment plan for static recrystallization.

Simulation Id	8	9
Initial mean energy by grains (MPa)		6.68
Initial mean grain size ( $\mu\text{m}$ )		0.22
Mean particles radius (nm)		5
Particles surface fraction %	0	1
Introduction of initial nuclei	yes	no

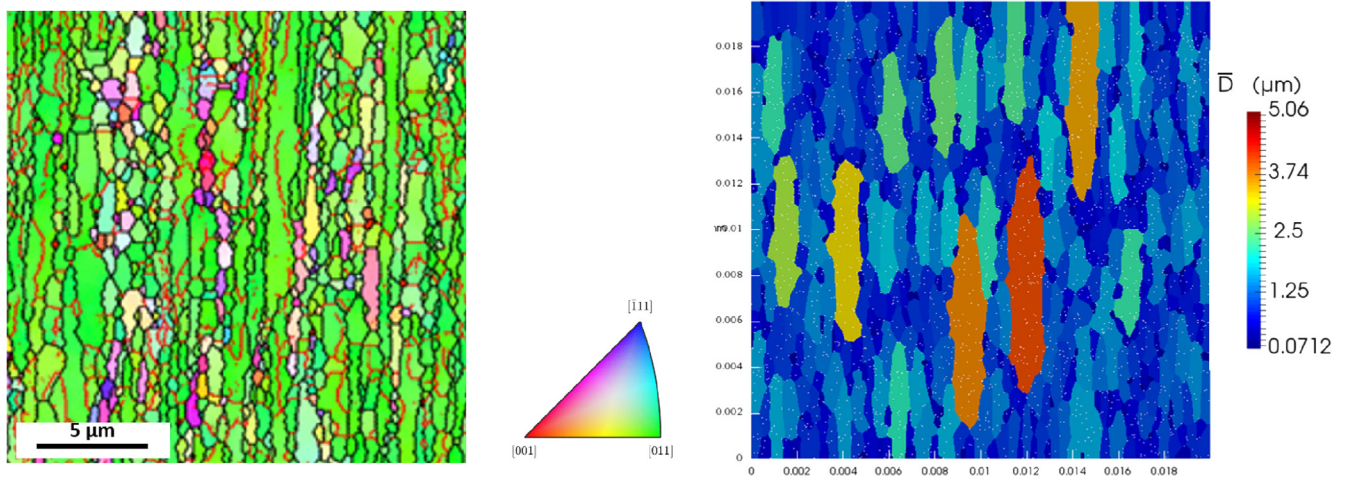


Fig. 8. Modelled microstructure at pinned state, with 0.5% of 10 nm particles in MC model (left side) and LS model (right side) ( $t = 0.2$  s for LS method and  $t = 20$  MCS for MC).

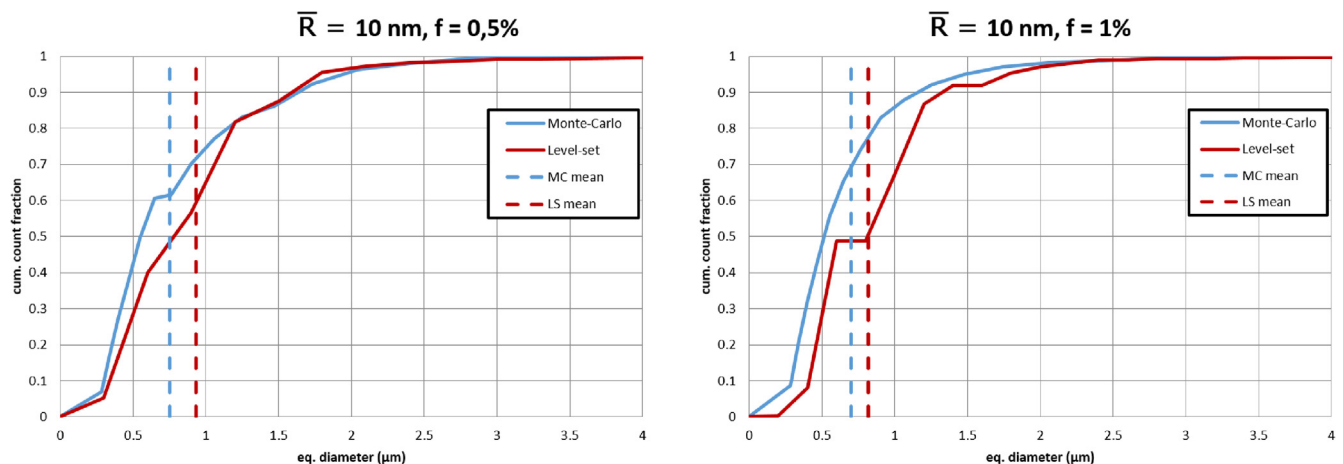


Fig. 9. Grain size distributions from LS and MC simulations at pinned state: (left side)  $t = 0.38$  s for  $f = 0.5\%$  and (right side)  $t = 0.2$  s for  $f = 1\%$ .

particles surface fraction (Fig. 9).

Even if the codes used here does not have the same maturity level (LS code is a parallelized commercial code and MC is a research and not parallelized code), it is interesting to compare the evolution of the computation time for each model, between a no-particles case to a case with almost 10 000 nanoparticles. For MC method, computation time remains quite the same with or without SPP (around 100 MCS in 1 day on a  $20 \times 20 \mu\text{m}^2$  map on a single processor) and particles size has only a small influence on it. That is why it is possible with this method to model microstructure evolution with particles smaller than 5 nm even if for such particles size the assumption “grain boundary thickness is negligible behind particles size” is questionable. For the LS method, introducing very small particles largely increases the computation time: with  $\bar{r} = 10$  nm and  $f = 0.5\%$  on a  $20 \times 20 \mu\text{m}^2$  map, 8 days on 20 processors are necessary to reach the pinned state at 0.2 s, where the same simulation without particles takes only few seconds. This difference between cases with and without particles in the LS method could be explained with two observations. First, introducing very small particles requires using mesh elements smaller than particles, small enough to describe their shape, so the total number of mesh elements increases massively (from around 162 000 without particles up to around 4 million with 0.5% of 10 nm particles). The other parameter that has a strong influence on calculation time in the LS framework is time step. The DIGIMU software [45], used here for the LS simulations, defines it automatically, considering grain boundary mobility, storage frequency and particles size. As particles are very small, grain boundaries

curvature could be very high around them, which lead to a high capillarity force and a smaller time step: around 9 300 time steps with 10 nm particles are necessary to reach 0.2 s, whereas only 160 time steps are needed without particles. It explains why it is difficult to model microstructure evolution with particles smaller than 5 nm in LS model.

#### 3.4. Effects of stored energy on microstructures: static recrystallization for cold deformed microstructure

After hot-extrusion, ODS steels bar need to be cold-deformed to give them their final shape. Then, in this section, recrystallization at  $T = 1423.15$  K after a cold forming process was simulated. In order to get closer from the real thermomechanical treatment, stored energy field are calculated from experimental data by considering KAM (Kernel Average Misorientation) gradient across the map such as described in [46,47]. For a precise comparison with MC simulations and experiments, it is important to use the stored energy field associated with the experimental maps (Fig. 10), so the dislocation density field measured from experimental data is directly immersed in LS simulations as described in Section 2.2.

The higher amount of stored energy and experimental observations, showing that crystallographic orientations are changed after annealing [42], suggest that a discontinuous recrystallization process occurs. It explains why, with this microstructure, a site-saturated nucleation step was considered. In case of site-saturated nucleation, the nuclei, free of

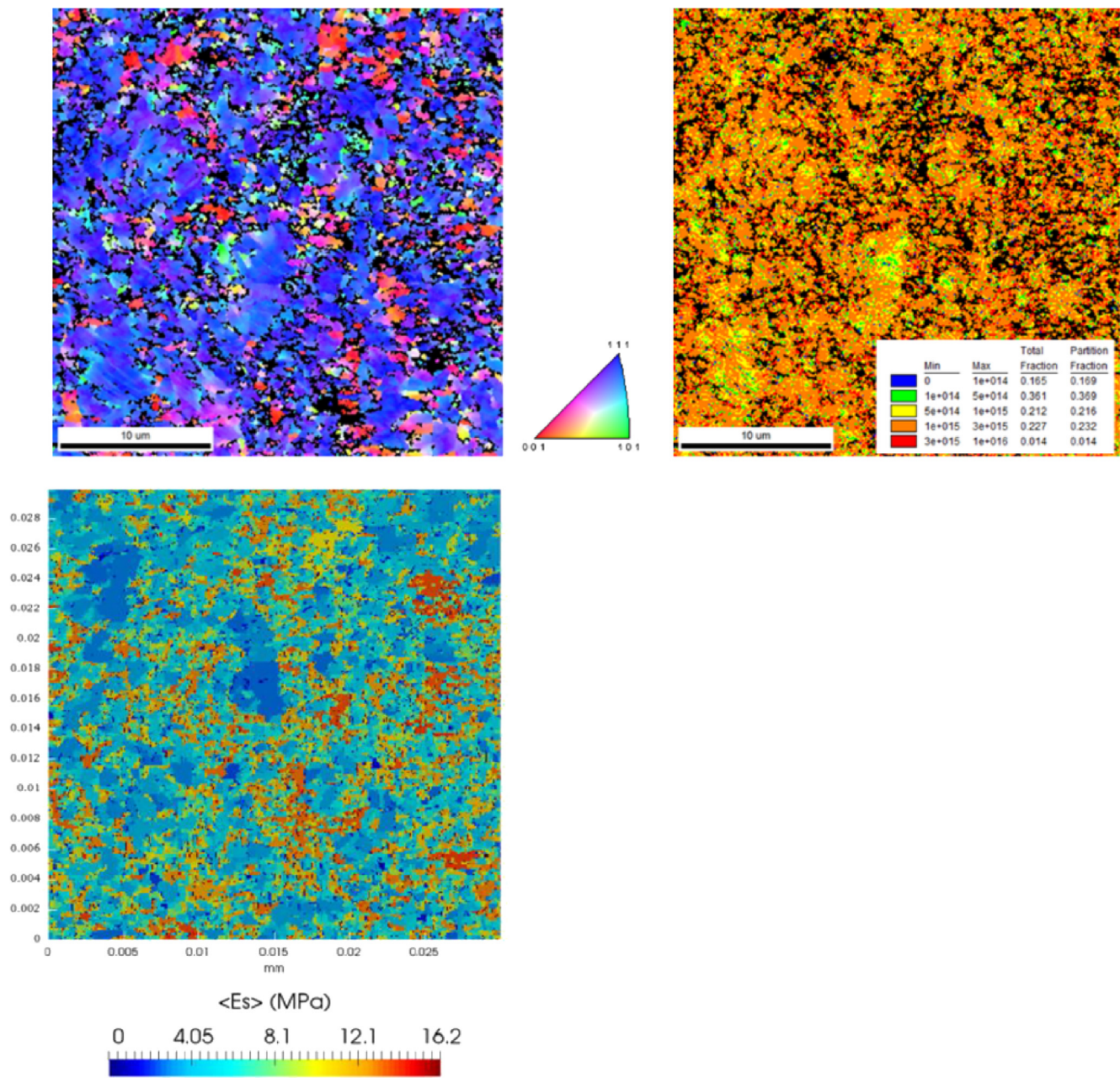


Fig. 10. EBSD map of initial cold deformed microstructure (top left), associated dislocation density field (top right), and LS polycrystal immersed from these data (bottom).

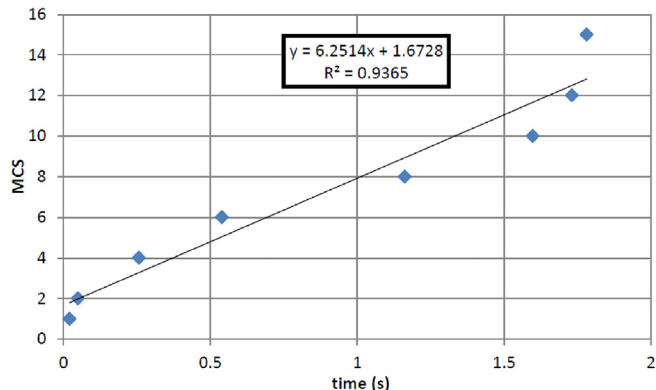
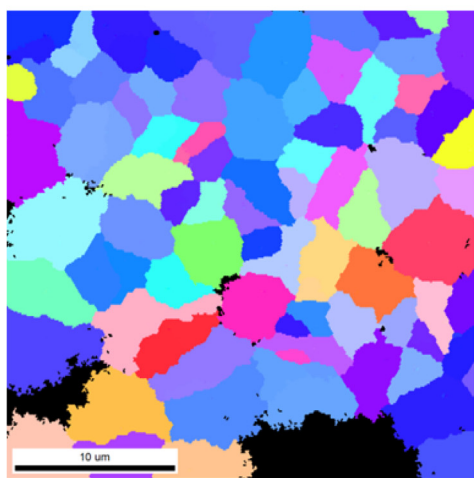
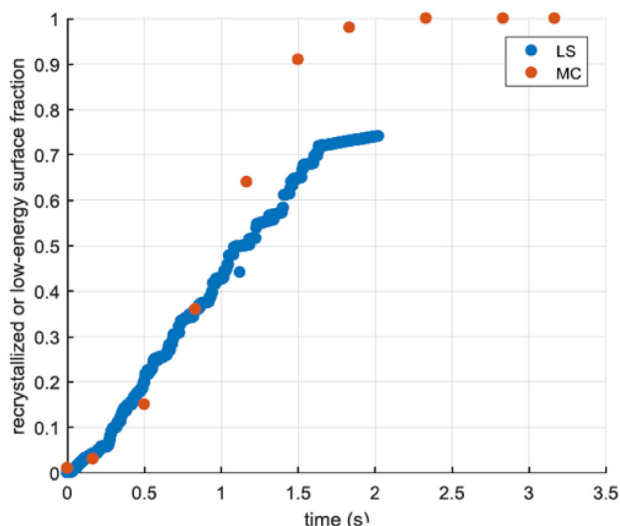


Fig. 11. Relationship between MCS and time by comparisons of recrystallized mean grain diameter.

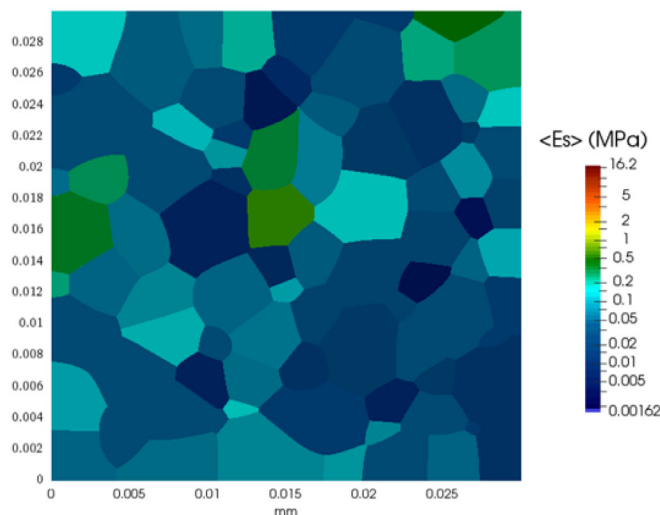
dislocations, are introduced in high-energy area with the same coordinates as in MC simulations. A dislocation density threshold sets their number. This threshold is chosen to meet the experimental recrystallized grain size. For this comparison,  $30 \times 30 \mu\text{m}^2$  experimental maps are used, with a resolution of  $0.1 \mu\text{m}$  in MC. In LS the corresponding initial mesh contains 5 612 000 elements due to the very small grain size of the microstructure.

An initial radius needs to be set for the nuclei. This initial radius should be high enough so that its stored energy could balance the capillarity forces induced by surrounding grains. As it is proposed in [25], a critical radius could be calculated with the Bailey-Hirsch criterion. Thus, the critical initial diameter for nuclei is set at  $D^* = 0.32 \mu\text{m}$ . In the MC model, the initial size for these nuclei is set to 1 pixel which corresponds to  $D_{MC} = 0.1 \mu\text{m}$ .

As expected, most nuclei disappear when they are introduced in LS simulations with such sizes. In MC simulations, nuclei could grow as



10 MCS



Time = 1.595 s

Fig. 12. Top: evolution of the recrystallized surface fraction modelled with MC and the low-energy surface fraction obtained in the LS simulation (simulation n° 8). Bottom: MC (left side) and LS (right side) simulation at 10 MCS (1.595 s), only recrystallized grains appears on MC simulation, recrystallized grains are in dark blue on LS simulation ( $E_s < 0.05$  MPa). MCS are converted into seconds with the relationship obtained in Fig. 11.

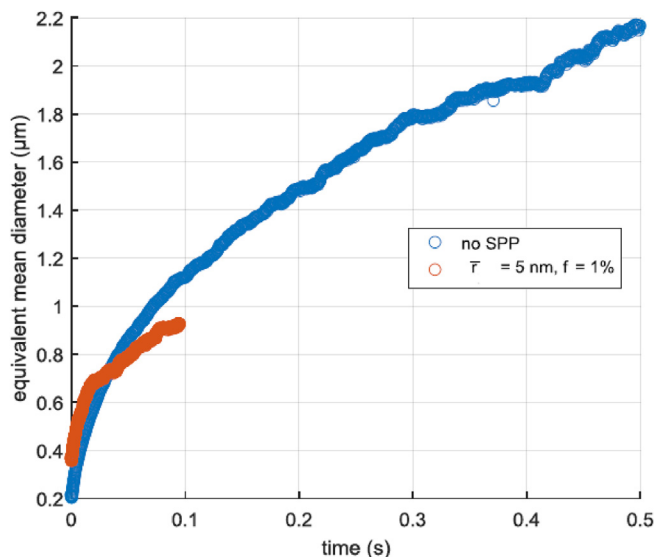


Fig. 13. Evolution of the equivalent mean diameter with stored energy, with and without SPP (LS simulations n° 8 and n° 9).

local curvature is not taken into account for them (migration of the non-recrystallized grains is neglected and the driving pressure for nuclei is chosen as only linked to the stored energy gradients). As for GG simulations with particles (see Section 3.3), these results illustrate that the capillarity force coming from grain boundary curvature is then underestimated in this model, so that small nuclei could grow even if their size are largely under the critical size. Nuclei, respecting an initial diameter equal to  $D^*$ , were introduced in LS simulations to model this discontinuous recrystallization phenomenon.

Results from simulation n° 8 could be compared with results from MC simulations. As in Section 3.1, MCS could be linked with time by comparing mean recrystallized grain diameter from MC simulations with mean low energy grain diameter from LS simulations (Fig. 11).

For this microstructure, the equivalence between MCS and time is around 6 MCS for 1 s. The relation between MCS and time seems to be irregular from a simulation to another, when recrystallization is modelled. We could wonder if these differences with the hot extruded microstructure are due to a different morphology of initial grain structure, a higher energy level or others parameters.

With this relation, it is possible to compare the evolution of the recrystallized surface fraction in MC and the low-energy grains in LS (see Fig. 12).

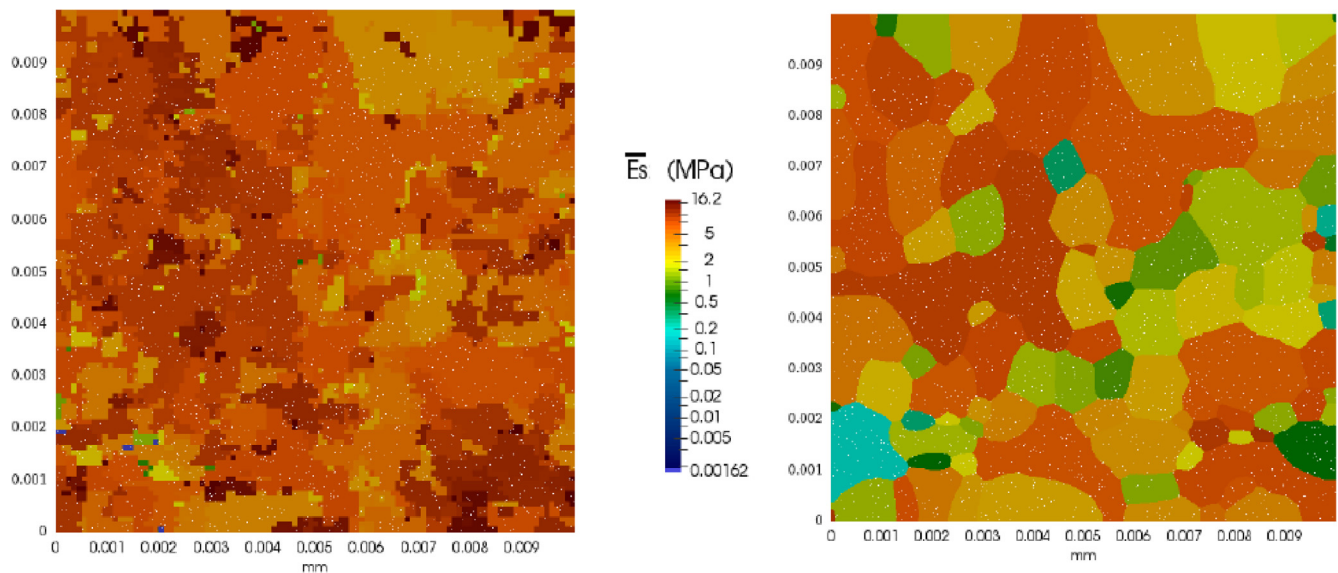


Fig. 14. Cold deformed microstructure with SPP (LS simulation n° 9,  $\bar{r} = 5$  nm and  $f = 1\%$ ), left: initial state, right: at  $t = 0.1$  s.

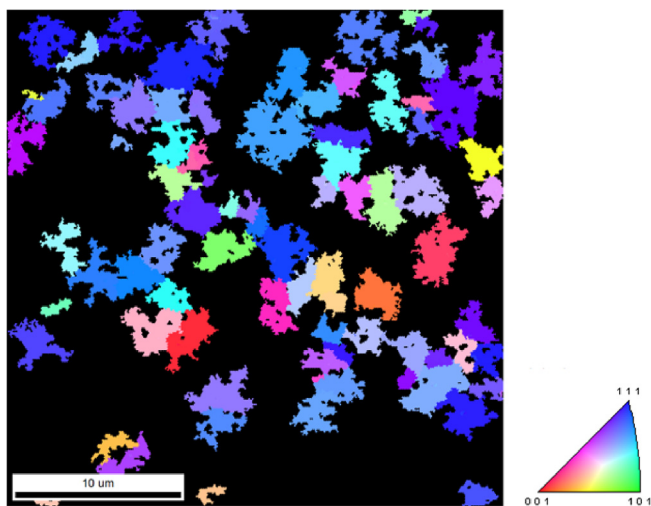


Fig. 15. Cold deformed microstructure with SPP (MC simulation,  $\bar{r} = 1.5$  nm and  $f = 0.5\%$ ), at 10 MCS.

Approximations done in MC where only the nuclei evolve seems to have few impact, leading to a global evolution close from the result observed in LS simulation where all the microstructure evolve. Indeed, large grains evolve much slower than small low energy grains present in the initial microstructure. Therefore, evolution of small grains is predominant in comparison to large grains.

As the stored energy has an impact on the maximum grain size obtained when particles are added, it is interesting to perform a LS simulation with 5 nm particles on this cold deformed microstructure (simulation n° 9).

Adding these SPP has less impact on the cold deformed microstructure evolution than with the hot extruded microstructure (see Fig. 13 comparatively to Fig. 5), this is due to the high stored energy which can partially balance the pinning force introduced by SPP. Then, at 0.1 s, the pinned state is not reached but some grains are already near a low energy level (Fig. 14). MC simulations with higher SPP fraction (Fig. 15) show also that it is possible to partially recrystallize this material. A higher recrystallized fraction at pinned state could be expected in these conditions. Longer simulations need to be performed to confirm this result. Then, experimental data show also that specimens with very small SPP, annealed after a cold forming process could be

partially recrystallized in these conditions [42].

Even if LS and MC numerical frameworks are using different assumptions to model recrystallization, they lead to the same behavior, such as for the cold deformed microstructures. Other simulations should be done to complete these first comparisons, such as longer LS simulations with nuclei, or MC simulations with 5 nm SPP. In the end, comparisons with experimental observations will determine which assumptions are more relevant to get closer to the reality.

#### 4. Conclusion and perspectives

- In simple grain growth case, a linear relationship between MCS and time is obtained, and grain size distributions are quite the same for the two models. Therefore, it is possible to use a LS method as a reference to calibrate a MC method.
- With micrometric particles size, simulations show good agreement with the available experimental values. This illustrates that involved physical mechanisms seem well described and that  $M$  and  $\gamma$  parameters seem well estimated. It illustrates also that grain boundary anisotropy and 3D effects seem to have a second order impact for this kind of pinned microstructure. Additional experiments must be carried out to substantiate this assertion.
- For particles sizes under 5 nm, results from LS simulations are not fully matching the Smith-Zener model and experimental values are no longer on the fit defined by the LS simulations and the Smith-Zener model. These observations suggest that other parameters such as crystallographic particles structure, particle's coherency or inter-atomic interactions should also be considered at this scale.
- With particles, the relation between MCS and time stays close to the one established without particles. A shift in the mean grain size at pinned state is observed between MC and LS results, which could be explained by an underestimation of the capillarity force in the MC model. Despite that, grain size distributions at pinned state are close from a model to another.
- For recrystallization, the link between MCS and time is different from the one obtained in simple grain growth cases. Evolution of recrystallized surface fraction shows good agreement for the cold deformed microstructure. Approximations done in MC, where only nuclei evolve, have a less important impact for this type of microstructure.
- With nanoparticles and stored energy, the limit grain size is

increased and dependent of the amount of stored energy. With a high amount of energy (cold deformation), it is possible to attain almost a fully recrystallized state.

These results show that strengths from MC method, such as the low calculation time whatever particles size and explicit cristallographic evolution, and strengths from LS method, such as the direct link with physical time and precision for interaction with particles, could be gathered by using few LS simulations to calibrate a MC model. Thus, fewer experiments on real materials are needed and calculation time could be saved.

However, some points remain unsolved. In this study, grains boundaries are described as sharp interfaces, but usual oxide precipitates in ODS steels are so small that their size can have the same order of magnitude than grain interface thickness. Under those facts, we could wonder if the physics laws used here to describe grain boundaries/oxides interactions are sufficient as no evolution of the SPPs during grain boundary migration is considered. More experiments and simulations with such particles sizes should be done to discuss this question.

#### Data availability

The raw/processed data required to reproduce these findings cannot be shared at this time due to legal or ethical reasons.

#### CRedit authorship contribution statement

**F. Villaret:** Methodology, Validation, Formal analysis, Investigation, Data curation, Writing - original draft, Visualization. **B. Hary:** Conceptualization, Investigation, Writing - review & editing. **Y. de Carlan:** Conceptualization, Writing - review & editing. **T. Baudin:** Conceptualization, Software, Writing - review & editing. **R. Logé:** Conceptualization, Writing - review & editing. **L. Maire:** Methodology, Conceptualization, Software. **M. Bernacki:** Methodology, Conceptualization, Software, Validation, Formal analysis, Investigation, Writing - original draft, Visualization, Supervision, Project administration, Funding acquisition.

#### Declaration of Competing Interest

The authors declare that they have no known competing financial interests or personal relationships that could have appeared to influence the work reported in this paper.

#### Acknowledgements

The authors thank the ArcelorMittal, ASCOMETAL, AUBERT & DUVAL, CEA, FRAMATOME, SAFRAN, TIMET, Constellium and TRANSVALOR companies and the ANR for their financial support through the DIGIMU consortium and ANR industrial Chair (Grant No. ANR-16-CHIN-0001).

#### References

- [1] P. Yvon, F. Carré, Structural materials challenges for advanced reactor systems, *J. Nucl. Mater.* 385 (2) (2009) 217–222, <https://doi.org/10.1016/j.jnucmat.2008.11.026> nuclear Materials III. <http://www.sciencedirect.com/science/article/pii/S0022311508007149>.
- [2] A. Alamo, V. Lambard, X. Averty, M. Mathon, Assessment of ods-14% cr ferritic alloy for high temperature applications, *J. Nucl. Mater.* 329 (2004) 333–337.
- [3] T. Chou, H. Bhadeshia, Recrystallization temperatures in mechanically alloyed oxide-dispersion-strengthened ma956 and ma957 steels, *Mater. Sci. Eng.: A* 189 (1) (1994) 229–233, [https://doi.org/10.1016/0921-5093\(94\)90419-7](https://doi.org/10.1016/0921-5093(94)90419-7) URL: <http://www.sciencedirect.com/science/article/pii/0921509394904197>.
- [4] D. Srolovitz, M. Anderson, G. Grest, P. Sahni, Computer simulation of grain growth-iii. influence of a particle dispersion, *Acta Metall.* 32 (9) (1984) 1429–1438, [https://doi.org/10.1016/0001-6160\(84\)90089-0](https://doi.org/10.1016/0001-6160(84)90089-0) URL <http://www.sciencedirect.com/science/article/pii/0001616084900890>.
- [5] M. Miodownik, E.A. Holm, G.N. Hassold, Highly parallel computer simulations of particle pinning: zener vindicated, *Scr. Mater.* 42 (12) (2000) 1173–1177, [https://doi.org/10.1016/S1359-6462\(00\)00354-7](https://doi.org/10.1016/S1359-6462(00)00354-7) URL: <http://www.sciencedirect.com/science/article/pii/S1359646200003547>.
- [6] D. Raabe, L. Hantcherli, 2d cellular automaton simulation of the recrystallization texture of an if sheet steel under consideration of zener pinning, *Comput. Mater. Sci.* 34 (4) (2005) 299–313, <https://doi.org/10.1016/j.commatsci.2004.12.067> URL: <http://www.sciencedirect.com/science/article/pii/S092702560500011X>.
- [7] G. Couturier, C. Maurice, R. Fortunier, Three-dimensional finite-element simulation of zener pinning dynamics, *Philos. Mag.* 83 (30) (2003) 3387–3405, <https://doi.org/10.1080/1478643031000152771>.
- [8] N. Moelans, B. Blanpain, P. Wollants, Phase field simulations of grain growth in two-dimensional systems containing finely dispersed second-phase particles, *Acta Mater.* 54 (4) (2006) 1175–1184, <https://doi.org/10.1016/j.actamat.2005.10.045> URL: <http://www.sciencedirect.com/science/article/pii/S1359645405006555>.
- [9] A. Agnoli, N. Bozzolo, R. Logé, J.-M. Franchet, J. Laigo, M. Bernacki, Development of a level set methodology to simulate grain growth in the presence of real secondary phase particles and stored energy – application to a nickel-base superalloy, *Comput. Mater. Sci.* 89 (2014) 233–241, <https://doi.org/10.1016/j.commatsci.2014.03.054> URL: <http://www.sciencedirect.com/science/article/pii/S0927025614002158>.
- [10] M. Anderson, D. Srolovitz, G. Grest, P. Sahni, Computer simulation of grain growth – I Kinetics, *Acta metallurgica* 32 (5) (1984) 783–791.
- [11] G. Grest, D. Srolovitz, M. Anderson, Computer simulation of grain growth – IV. Anisotropic grain boundary energies, *Acta Metallurgica* 33 (3) (1985) 509–520.
- [12] D. Srolovitz, G. Grest, M. Anderson, Computer simulation of grain growth –V Abnormal grain growth, *Acta Metallurgica* 33 (12) (1985) 2233–2247.
- [13] D. Srolovitz, G. Grest, M. Anderson, A. Rollett, Computer simulation of recrystallization –II. Heterogeneous nucleation and growth, *Acta metallurgica* 36 (8) (1988) 2115–2128.
- [14] A. Rollett, D.J. Srolovitz, M. Anderson, R. Doherty, Computer simulation of recrystallization –III. Influence of a dispersion of fine particles, *Acta metallurgica et materialia* 40 (12) (1992) 3475–3495.
- [15] A. Rollett, M. Luton, D.J. Srolovitz, Microstructural simulation of dynamic recrystallization, *Acta metallurgica et materialia* 40 (1) (1992) 43–55.
- [16] P. Peczak, A monte carlo study of influence of deformation temperature on dynamic recrystallization, *Acta Metall. Mater.* 43 (3) (1995) 1279–1291.
- [17] S. Osher, J.A. Sethian, Fronts propagating with curvature-dependent speed: algorithms based on Hamilton-Jacobi formulations, *J. Comput. Phys.* 79 (1) (1988) 12–49, [https://doi.org/10.1016/0021-9991\(88\)90002-2](https://doi.org/10.1016/0021-9991(88)90002-2) URL: <http://www.sciencedirect.com/science/article/pii/0021999188900022>.
- [18] B. Merriman, J.K. Bence, S.J. Osher, Motion of multiple junctions: a level set approach, *J. Comput. Phys.* 112 (2) (1994) 334–363, <https://doi.org/10.1006/jcph.1994.1105> URL: <http://linkinghub.elsevier.com/retrieve/pii/S0021999184711053>.
- [19] H.-K. Zhao, T. Chan, B. Merriman, S. Osher, A variational level set approach to multiphase motion, *J. Comput. Phys.* 127 (1) (1996) 179–195.
- [20] M. Bernacki, Y. Chastel, T. Coupez, R.E. Logé, Level set framework for the numerical modelling of primary recrystallization in polycrystalline materials, *Scr. Mater.* 58 (12) (2008) 1129–1132, <https://doi.org/10.1016/j.scriptamat.2008.02.016> URL: <http://www.sciencedirect.com/science/article/pii/S1359646208001425>.
- [21] M. Bernacki, H. Resk, T. Coupez, R.E. Logé, Finite element model of primary recrystallization in polycrystalline aggregates using a level set framework, *Modell. Simul. Mater. Sci. Eng.* 17 (6) (2009) 064006 URL: <http://stacks.iop.org/0965-0393/17/i=6/a=064006>.
- [22] M. Bernacki, R.E. Logé, T. Coupez, Level set framework for the finite-element modelling of recrystallization and grain growth in polycrystalline materials, *Scr. Mater.* 64 (6) (2011) 525–528, <https://doi.org/10.1016/j.scriptamat.2010.11.032> URL: <http://www.sciencedirect.com/science/article/pii/S1359646210007906>.
- [23] B. Scholtes, R. Boulais-Sinou, A. Settefrati, D. Pino Muñoz, I. Poitraul, A. Montouchet, N. Bozzolo, M. Bernacki, 3D level set modeling of static recrystallization considering stored energy fields, *Comput. Mater. Sci.* 122 (2016) 57–71 URL <http://linkinghub.elsevier.com/retrieve/pii/S0927025616302142>.
- [24] H. Hallberg, A modified level set approach to 2d modeling of dynamic recrystallization, *Modell. Simul. Mater. Sci. Eng.* 21 (8) (2013) 085012 URL: <http://stacks.iop.org/0965-0393/21/i=8/a=085012>.
- [25] L. Maire, B. Scholtes, C. Moussa, N. Bozzolo, D. Pino Muñoz, A. Settefrati, M. Bernacki, Modeling of dynamic and post-dynamic recrystallization by coupling a full field approach to phenomenological laws, *Mater. Des.* 133 (Supplement C) (2017) 498–519, <https://doi.org/10.1016/j.matdes.2017.08.015> URL <http://www.sciencedirect.com/science/article/pii/S026412751730761X>.
- [26] A. Agnoli, N. Bozzolo, R. Logé, J.-M. Franchet, J. Laigo, M. Bernacki, Development of a level set methodology to simulate grain growth in the presence of real secondary phase particles and stored energy –application to a nickel-base superalloy, *Comput. Mater. Sci.* 89 (2014) 233–241.
- [27] B. Scholtes, D. Ilin, A. Settefrati, N. Bozzolo, A. Agnoli, M. Bernacki, Full field modeling of the Zener pinning phenomenon in a level set framework – discussion of classical limiting mean grain size equation, *Superalloys 2016: Proceedings of the 13th International Symposium on Superalloys*, 2016, pp. 497–503.
- [28] M. Eleyse, S. Eshedoglu, P. Smereka, Diffusion generated motion for grain growth in two and three dimensions, *J. Comput. Phys.* 228 (21) (2009) 8015–8033, <https://doi.org/10.1016/j.jcp.2009.07.020> URL: <http://www.sciencedirect.com/science/article/pii/S0021999109004082>.
- [29] C. Mießner, M. Liesenjohann, L. Barrales-Mora, L. Shvindlerman, G. Gottstein, An

- advanced level set approach to grain growth – accounting for grain boundary anisotropy and finite triple junction mobility, *Acta Materialia* 99 (Supplement C) (2015) 39–48, <https://doi.org/10.1016/j.actamat.2015.07.040>.
- [30] J. Fausty, N. Bozzolo, M. Bernacki, A 2d level set finite element grain coarsening study with heterogeneous grain boundary energies, *Appl. Math. Model.* 78 (2020) 505–518, <https://doi.org/10.1016/j.apm.2019.10.008> URL: <http://www.sciencedirect.com/science/article/pii/S0307904X19305967>.
- [31] D. Ilin, N. Bozzolo, T. Toulorge, M. Bernacki, Full field modeling of recrystallization: effect of intragranular strain gradients on grain boundary shape and kinetics, *Comput. Mater. Sci.* 150 (2018) 149–161, <https://doi.org/10.1016/j.commatsci.2018.03.063> URL: <http://www.sciencedirect.com/science/article/pii/S0927025618302222>.
- [32] J. Humphreys, G.S. Rohrer, A. Rollett, Chapter 5 – mobility and migration of boundaries, in: J. Humphreys, G.S. Rohrer, A. Rollett (Eds.), *Recrystallization and Related Annealing Phenomena*, third ed., Elsevier, Oxford, 2017, pp. 145–197 URL <https://www.sciencedirect.com/science/article/pii/B9780080982359000057>.
- [33] B. Scholtes, M. Shakoov, A. Settefrati, P.-O. Bouchard, N. Bozzolo, M. Bernacki, New finite element developments for the full field modeling of microstructural evolutions using the level-set method, *Comput. Mater. Sci.* 109 (2015) 388–398, <https://doi.org/10.1016/j.commatsci.2015.07.042> URL: <http://www.sciencedirect.com/science/article/pii/S0927025615004528>.
- [34] M. Shakoov, B. Scholtes, P.-O. Bouchard, M. Bernacki, An efficient and parallel level set reinitialization method – application to micromechanics and microstructural evolutions, *Appl. Math. Model.* 39 (23) (2015) 7291–7302, <https://doi.org/10.1016/j.apm.2015.03.014> URL: <http://www.sciencedirect.com/science/article/pii/S0307904X15001638>.
- [35] A. Agnoli, M. Bernacki, R. Logé, J.-M. Franchet, J. Laigo, N. Bozzolo, Selective growth of low stored energy grains during  $\delta$ sub-solvus annealing in the inconel 718 nickel base superalloy, *Metall. Mater. Trans. A* 46 (9) (2015) 4405–4421.
- [36] T. Baudin, P. Paillard, R. Penelle, Grain growth simulation starting from experimental data, *Scr. Mater.* 36 (7) (1997) 789–794, [https://doi.org/10.1016/S1359-6462\(96\)00451-4](https://doi.org/10.1016/S1359-6462(96)00451-4) URL: <http://www.sciencedirect.com/science/article/pii/S1359646296004514>.
- [37] W. Wang, A.L. Helbert, F. Brisset, M.H. Mathon, T. Baudin, Monte Carlo simulation of primary recrystallization and annealing twinning, *Acta Mater.* 81 (2014) 457–468, <https://doi.org/10.1016/j.actamat.2014.08.032>.
- [38] W.T. Read, W. Shockley, Dislocation models of crystal grain boundaries, *Phys. Rev.* 78 (3) (1950) 275, <https://doi.org/10.1103/PhysRev.78.275>.
- [39] A.R. Eivani, J. Zhou, J. Duszczuk, A new approach to incorporating the effect of nano-sized dispersoids on recrystallization inhibition into Monte Carlo simulation, *Comput. Mater. Sci.* 54 (2012) 370–377, <https://doi.org/10.1016/j.commatsci.2011.10.016> URL: <http://www.sciencedirect.com/science/article/pii/S0927025611005854>.
- [40] M.A. Miodownik, A review of microstructural computer models used to simulate grain growth and recrystallisation in aluminium alloys, *J. Light Met.* 2 (3) (2002) 125–135, [https://doi.org/10.1016/S1471-5317\(02\)00039-1](https://doi.org/10.1016/S1471-5317(02)00039-1) URL: <http://www.sciencedirect.com/science/article/pii/S1471531702000391>.
- [41] L.E. Murr, *Interfacial phenomena in metals and alloys*, Addison-Wesley Pub. Co., Advanced Book Program, United States, 1975. URL: [https://inis.iaea.org/search/search.aspx?orig\\_q=RN:7236335](https://inis.iaea.org/search/search.aspx?orig_q=RN:7236335).
- [42] B. Hary, *Investigation and modelling of the influence of nano-oxides concentration and deformation texture on the recrystallization of ferritic ODS steels*, Université Paris Saclay, 2017 (Ph.D. thesis).
- [43] C.C. Eiselt, H. Schendzielorz, A. Seubert, B. Hary, Y. de Carlan, P. Diano, B. Perrin, D. Cedat, ODS-materials for high temperature applications in advanced nuclear systems, *Nucl. Mater. Energy* 9 (2016) 22–28, <https://doi.org/10.1016/j.nme.2016.08.017> URL: <http://www.sciencedirect.com/science/article/pii/S2352179115300983>.
- [44] J. Zhou, C. Li, M. Guan, F. Ren, X. Wang, S. Zhang, B. Zhao, Zener pinning by coherent particles: pinning efficiency and particle reorientation mechanisms, *Modell. Simul. Mater. Sci. Eng.* 25 (6) (2017) 065008, <https://doi.org/10.1088/1361-651x/aa6cfb>.
- [45] P. De Micheli, L. Maire, D. Cardinaux, C. Moussa, N. Bozzolo, M. Bernacki, Digimu full field recrystallization simulations for optimization of multi-pass processes, *Proceedings of the 22nd International ESAFORM Conference on Material Forming*, 2019.
- [46] Y. Ateba Betanda, A.L. Helbert, F. Brisset, M.H. Mathon, T. Waeckerlé, T. Baudin, Measurement of stored energy in Fe-48%Ni alloys strongly cold-rolled using three approaches: neutron diffraction, Dillamore and KAM approaches, *Mater. Sci. Eng. A* 614 (2014) 193–198, <https://doi.org/10.1016/j.msea.2014.07.037>.
- [47] M. Kamaya, Assessment of local deformation using EBSD: Quantification of accuracy of measurement and definition of local gradient, *Ultramicroscopy* 111 (8) (2011) 1189–1199, <https://doi.org/10.1016/j.ultramic.2011.02.004>.